Journal of Materials Science: Materials in Electronics (2019) 30:15413–15419
https://doi.org/10.1007/s10854-019-01916-7

Structure, electrical, dielectric and ferroelectric properties of $(1-x)BiFeO_3-xAl_2O_3$ ceramics

Peijia Bai[1] · Yiming Zeng[1] · Jiao Han[1] · Yongxing Wei[2] · Mingwei Li[1] · Yutong Li[1]

Received: 26 May 2019 / Accepted: 20 July 2019 / Published online: 27 July 2019

Abstract
Lead-free ferroelectric composite ceramics of $(1-x)BiFeO_3-xAl_2O_3$ ($x=0.00$, 0.02, 0.04, 0.06, 0.08 and 0.10) were synthesized using the traditional solid-state reaction method. The effects of Al_2O_3 addition on structural (crystal data and microstructure), ferroelectric, dielectric properties, and leakage current characteristic were investigated. X-ray diffraction and scanning electron microscopy demonstrated that the addition of Al_2O_3 promoted the formation of the secondary phases ($Bi_2Fe_4O_9$ and $Bi_{24}Al_2O_{39}$) and the average grain size significantly reduced from 1.49 μm for $x=0.00$ to 0.45 μm for $x=0.10$. The samples with Al_2O_3 addition had lower dielectric constant and dielectric loss. The Curie temperature (T_C) decreased gradually from 475 °C for $x=0.02$ to 390 °C for $x=0.10$. Leakage current density decreased significantly with the addition of the Al_2O_3, and the leakage conduction mechanism was changed from Ohmic relationship to space charge limited conduction (SCLC) mechanism. The ferroelectric hysteresis loops became more typical in shape with the addition of the Al_2O_3.

1 Introduction

In order to promote the development of sensors, electrical transformers and high energy storage density devices, multiferroic materials have received much attention in recent decades [1, 2]. All multiferroic materials coexist of two or more ferroics (ferroelectric, ferromagnetic, and ferroelastic) [3, 4], providing an extra degree of freedom in practical applications. However, most multiferroic materials exhibit weak magneto-electric coupling effect and lose ferroelectric properties above room temperature [5, 6]. Therefore, it is a growing demand for developing a special material with high T_C and excellent magneto-electric coupling effect.

Among various multiferroics, $BiFeO_3$ (BFO) is the best choice for meeting those demands of device application, owing to its high ferroelectric Curie temperature ($Tc\approx830$ °C) and anti-ferromagnetic Néel temperature ($T_N\approx370$ °C) [7, 8]. $BiFeO_3$ has anti-ferromagnetic G-type of spin configuration character along $[111]_{cubic}$ or $[001]_{hexagonal}$ direction with pseudocubic or rhombohedral symmetry at room temperature [9]. With the $6s^2$ lone pair electron configuration of the Bi^{3+} ions and the partially filled d orbital of the Fe^{3+} ions, $BiFeO_3$ has great ferroelectric and ferromagnetic properties, respectively [10, 11]. However, $BiFeO_3$ has some inherent defects that limit its utilization in industry application. For instance, $BiFeO_3$ exhibits serious leakage current characteristic, which stems from the volatilization of Bi_2O_3 [8], the reduction of Fe^{3+} [6] and the generation of secondary phase ($Bi_2Fe_4O_9$ and $Bi_{25}FeO_{39}$) at sintering process [12, 13]. Besides, it also has a high dielectric loss and temperature instability. Thus, the greatest challenge for $BiFeO_3$ system is how to increase the ferroelectric properties and reduce leakage current density to promote its practical application.

By now, several attempts had been performed in the last decade to overcome these shortcomings of $BiFeO_3$ systems, such as substituting Bi-site by rare-earth ions [9], substituting Fe-site by transition-metal ions [2], fabricating its composites with another ABO_3-type perovskite materials [6] and so on. Among them, fabricating composites and solid solutions with other oxides can suppress the impurity phases and show outstanding ferroelectric properties. Zhuang et al. [11] synthesized Dy-modified $BiFeO_3$–$PbTiO_3$ multiferroics ceramics and found that the magnetic morphotropic phase boundary (MPB) in the $0.66Bi_{1-x}Dy_xFeO_3-0.34PbTiO_3$

✉ Yiming Zeng
zengym0871@126.com

[1] State Key Laboratory of Advanced Technologies for Comprehensive Utilization of Platinum Metals, Kunming Institute of Precious Metals, Kunming 650106, People's Republic of China

[2] School of Materials and Chemical Engineering, Xi'an Technological University, Xi'an 710021, China

system, which significantly enhanced the dielectric and ferromagnetic performances of $BiFeO_3$ system. Wei et al. [12] fabricated $(1-x)BiFeO_3-xBaTiO_3$ composite ceramics using the traditional solid-state sintering route and observed that the highest remnant polarization ($P_r = 26.0\ \mu C/cm^2$) at $x = 0.3$, however, the P_r decreased from 26.0 $\mu C/cm^2$ for $x = 0.3$ to 8.2 $\mu C/cm^2$ for $x = 0.45$, meaning that excessive $BaTiO_3$ addition will decrease the ferroelectric properties of $BiFeO_3$. Jawad et al. [14] prepared $Bi_{1-x}Al_{2x}Fe_{1-x}O_3$ ceramics via a solution combustion method and demonstrated that the replacement of Al^{3+} at both sites created more oxygen vacancy, which resulted in an anomalous phenomenon in structural and resistivity, respectively. Azam et al. [15] synthesized the $Bi_{1-x}Al_{2x}Fe_{1-x}O_3$ ceramics and found that the activation energies increased from 0.54 to 0.73 eV with the addition of Al. However, the $BiFeO_3$-Al_2O_3 composite ceramics has received comparatively less attention.

In this study, the addition oxide Al_2O_3 was applied to form composite ceramics with $BiFeO_3$, and the effects of Al_2O_3 addition on structural (crystal data and microstructure), leakage current characteristic, ferroelectric and dielectric properties of $(1-x)BiFeO_3-xAl_2O_3$ composite ceramics were investigated.

2 Experimental details

$(1-x)BiFeO_3-xAl_2O_3$ composite ceramics, where $x = 0.00$, 0.02, 0.04, 0.06, 0.08 and 0.10 (denoted as A0, A2, A4, A6, A8 and A10, respectively), were prepared via the solid-state sintering route. The high purity (≥ 99%) starting reagents of Fe_2O_3, Al_2O_3, and Bi_2O_3 (all from Sinopharm Group Co., Ltd.) were used in this experiment. The oxides of Fe_2O_3 and Bi_2O_3 were accurately weighed in the stoichiometric proportion of $BiFeO_3$, the above ingredients were thoroughly mixed in the air for 1 h. The mixed powders were placed in alumina for calcining at 810° C for 2 h. The calcined bulks were again ground by ball milling for 12 h at a rate of 400 rpm with ethanol as a solvent. Then, the powder was sieved through 400 meshes and dried. The treated powder ($BiFeO_3$) was thoroughly mixed with Al_2O_3 in the above ratio. Finally, the powders were uniaxially pressed under a pressure of 50 MPa to obtain the green disk samples with 10 mm diameter and 1–2 mm thickness and then sintered at 780 °C for 2 h. In order to reduce the volatilization of Bi_2O_3, all compacted pellets were placed in a sealed alumina crucible during the sintering process.

The phase purity and structure for $(1-x)BiFeO_3-xAl_2O_3$ were detected by room temperature X-ray diffraction using a Rigaku diffractometer with Cu–Kα radiation (D/max-RB, Rigaku, Japan) The morphology of the sintered ceramics was evaluated via the scanning electron micrograph (SEM, TM-1000, Hitachi, Japan). Determination of relative density of all $(1-x)BiFeO_3-xAl_2O_3$ samples by Archimedes method. The sintered pellets were polished, electroded with silver-conductive paste on both parallel faces and fired at 550 °C for 15 min for electrical measurements. The electrical parameters of all the samples were measured in temperatures (25–500 °C) f and frequency (5×10^2–10^8 Hz) by an impedance analyzer (Agilent 4294A, America). The leakage current density and polarization hysteresis loops were evaluated using a ferroelectric tester (Ferroelectric analyzer, TF2000, Germany).

3 Results and discussion

The XRD Patterns for all the $(1-x)BiFeO_3-xAl_2O_3$ samples at room temperature are shown in Fig. 1. The diffraction peaks of all the samples were well-indexed with the JCPDS Card No: 86-1518 [16], indicating all the samples were rhombohedrally distorted perovskite structure with space group R3c. However, secondary phase diffraction peaks ($Bi_2Fe_4O_9$ and $Bi_{24}Al_2O_{39}$) became more pronounced with the increase of the Al_2O_3 content, indicating that the addition of Al_2O_3 increased the formation of secondary phases during the sintering process. In addition, there were no diffraction peaks matched with Al_2O_3 (JCPDS Card No: 10-0173) in all samples, indicating that Al_2O_3 participated in the reaction to form $Bi_{24}Al_2O_{39}$, and the residual content of Al_2O_3 lower than the limit detection of XRD. An enlarged view of patterns in the 2θ range of 31.5°–32.5° and the lattice parameter of all the samples are displayed in Fig. 1b and Table 1, respectively. The results showed that with the increase of the Al_2O_3 content, there was no obvious major peak shifted, and the lattice parameter had little changed, indicating that the Al^{3+} did not enter the $BiFeO_3$ lattice position [17]. As an unstable phase structure, $BiFeO_3$ easily decomposed in the temperature range of 447–831 °C [18], so the $Bi_{24}Al_2O_{39}$ may be produced by the interaction between $BiFeO_3$ and Al_2O_3 during the sintering process.

Figure 2 shows the cross-sectional SEM image for all the $(1-x)BiFeO_3-xAl_2O_3$ samples. It can be observed that the microstructure of the samples was changed with the increase of Al_2O_3 content. The pure $BiFeO_3$ sample presented that the grain had an irregular shape with an average grain size of 1.49 μm, and a large number of pores existed in some large grains owing to that rapid grain growth in the sintering process. With the increase of the Al_2O_3 content, the grain morphology changed to a more uniform distribution with obviously decreased in average grain size (0.45 μm of A10 samples), and the microstructures become denser, indicating that the addition of Al_2O_3 inhibited the growth of $BiFeO_3$ grain. It was possibly owing to the formation of secondary phases and the more refractory nature of Al_2O_3 [19]. In the A8 and A10 samples, there were many small grains attached

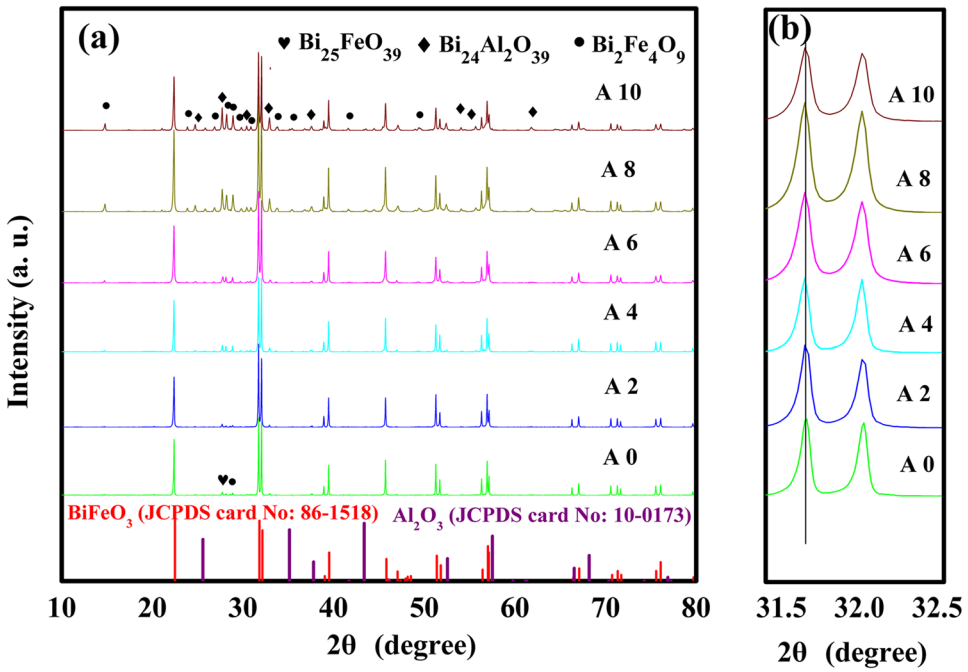

Fig. 1 RT XRD patterns for the $(1-x)BiFeO_3-xAl_2O_3$ samples

Table 1 The lattice parameters and volume for the $(1-x)BiFeO_3-xAl_2O_3$ samples

Samples	Lattice constant (Å)		Volume (V) in Å^3
	a	c	
A0	5.57715	13.86468	373.48
A2	5.57914	13.8697	373.88
A4	5.57848	13.86845	373.76
A6	5.57896	13.86888	373.83
A8	5.57868	13.86885	373.80
A10	5.57866	13.8693	373.81

around large grains, which caused the improvement of relative density from 89% for A0 to 93% for A10. High density and small grain size in bulk ceramics were believed to result in low leakage current density.

Figure 3 showed the variation of dielectric constant (ε_r) and dielectric loss (tan δ) depended on frequency dependence (5×10^2–10^8 Hz) for all the $(1-x)BiFeO_3-xAl_2O_3$ samples at room temperature. It can be observed that the magnitude of the permittivity of all the samples decreased with the increase of the frequency and became almost constant at high frequency. The high value of permittivity value at low frequency may be owing to the existed of different types of polarization factors, such as the and dipole moments, electronic and interfacial dislocations which were active in the low-frequency range. In addition, the dipole cannot follow high-frequency electric reversal. So, the value of high-frequency permittivity was less than that of the low-frequency one. [20]. At 10^6 Hz, the dielectric constant decreased monotonically with the increase of the Al_2O_3 content, maybe owing to the permittivity values of Al_2O_3 ($\varepsilon_r=9$) [21] and $Bi_2Fe_4O_9$ ($\varepsilon_r=23$) [22] were less than pure $BiFeO_3$ ($\varepsilon_r=96$) [17]. The value of dielectric loss reduced drastically with the increase in frequency within the tested range, due to the loss of space charge polarization at high-frequency range [23, 24]. In Al_2O_3 addition ceramics, the dielectric loss increases with the increase of Al_2O_3 content. It is owing to the formation of more impurity phases in the sintering process. However, the dielectric loss of Al_2O_3 addition ceramics was less than pure $BiFeO_3$ sample. This significant decreased in dielectric loss can be attributed to the denser structure observed in the SEM images which were beneficial for the dielectric properties of $BiFeO_3$ based ceramics.

The dielectric constant and dielectric loss as a function of temperature (25–500 °C) for the $(1-x)BiFeO_3-xAl_2O_3$ samples at 1 MHz is illustrated in Fig. 4. All the Al_2O_3 addition samples presented a dielectric constant ε (T) peak. With the addition of the Al_2O_3, the T_C decreased gradually from 475 °C for A2 to 390 °C for A10, the dielectric constant value decreased and the shape ε (T) peak became broad, it is owing to the generation of secondary phases and the increase of dielectric relaxor behavior in $(1-x)BiFeO_3-xAl_2O_3$ samples. Despite these changes, the value of the dielectric loss was small at less than 350 °C, but then it suddenly increased in higher temperature range, revealing an improvement in dc conductivity at high temperature. The rapid increase of dielectric loss at high temperature may be related to the release of space charge [25].

Figure 5 illustrates the room temperature leakage current density (J) as a function of applied voltages from −1000 to

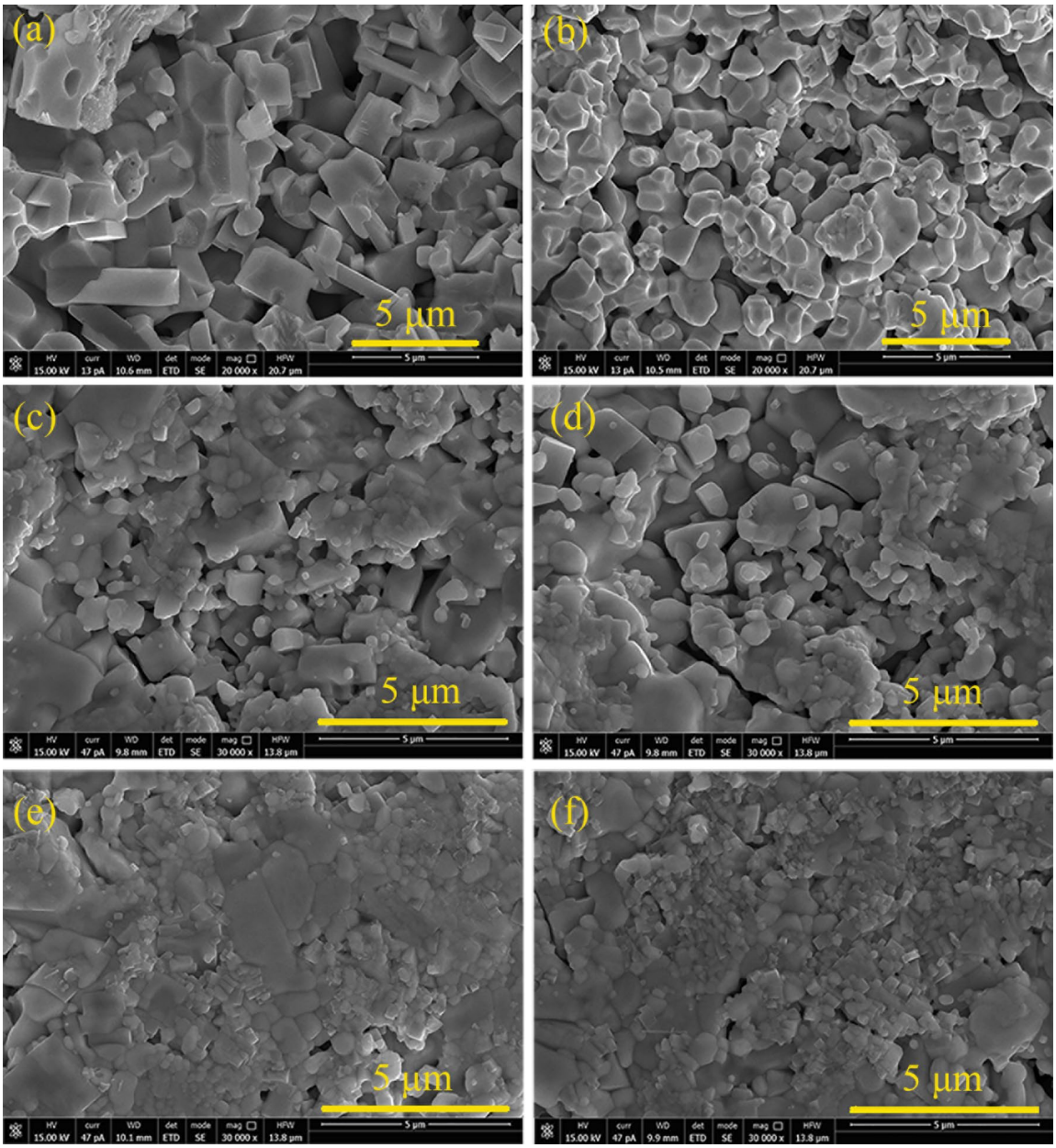

Fig. 2 SEM images for the $(1-x)BiFeO_3-xAl_2O_3$ samples: **a** A0, **b** A2, **c** A4, **d** A6, **e** A8, amd **f** A10

1000 V for all the $(1-x)BiFeO_3-xAl_2O_3$ samples. Leakage current density was decreased significantly with the addition of Al_2O_3. The observed leakage current densities for the $(1-x)BiFeO_3-xAl_2O_3$ samples were 8.01×10^{-6}, 6.38×10^{-6}, 1.30×10^{-6}, 3.75×10^{-7}, 1.97×10^{-7}, 9.18×10^{-8} A/cm^2 respectively at an applied voltage of 1000 V. The values demonstrated that leakage current density for A10 sample was decreased by about two orders of magnitude in comparison with pure $BiFeO_3$ sample. The fine grains and the compact structure had a close relationship with the decrease of the leakage current density for $(1-x)BiFeO_3-xAl_2O_3$ samples. The charges easily accumulated around the grain boundary to form small regions to increase resistance for ceramic. So, the decreased of the grain size will increase of the grain boundaries and resulted in a decrease in the leakage current density [26, 27] The leakage conduction mechanism can be used to explain the decrease of leakage current caused by the addition of Al_2O_3. Figure 6 shows the plot of log (J)–log (E) for $(1-x)BiFeO_3-xAl_2O_3$ samples at the positive voltage. The plots of A0, A2, and A4 showed a linear behavior with a slope of approximately 1, revealing an Ohmic relationship conduction behavior [28]. However, with the increases of the Al_2O_3 content, the A6, A8 and, A10 samples showed a linear behavior with a slope of 2 in

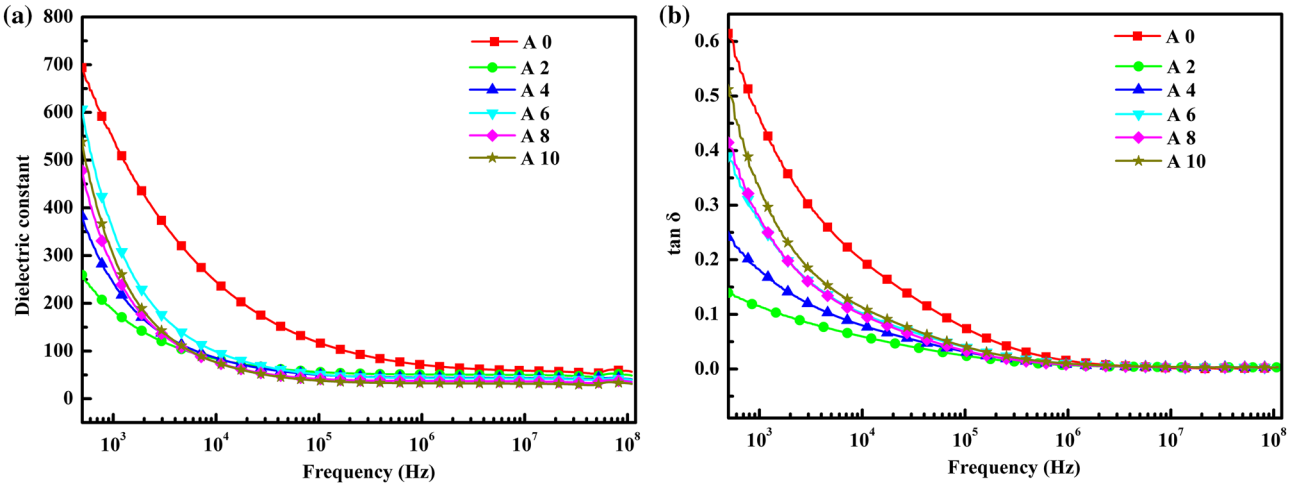

Fig. 3 Frequency dependence of dielectric parameters for the $(1-x)BiFeO_3-xAl_2O_3$ samples at RT: **a** ε_r and **b** tanδ

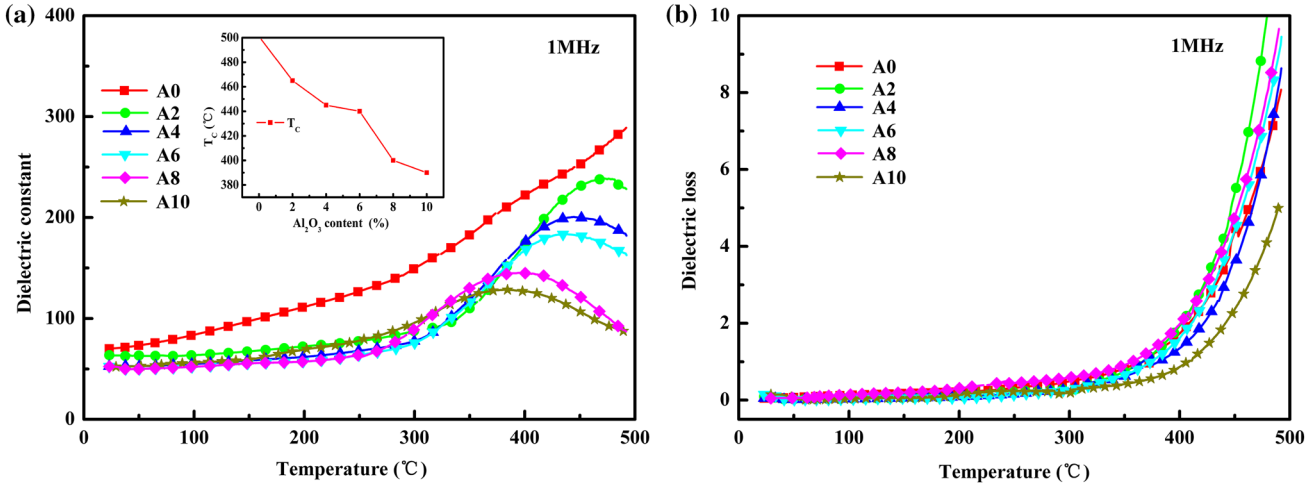

Fig. 4 Temperature dependence of dielectric parameters for the $(1-x)BiFeO_3-xAl_2O_3$ samples at 1 MHz: **a** ε_r and **b** tan δ

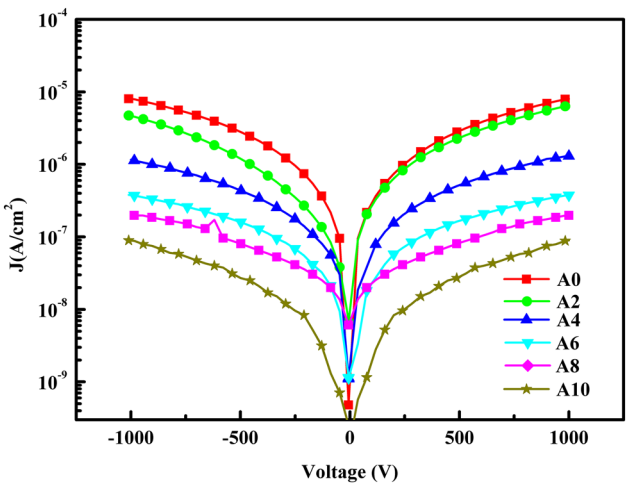

Fig. 5 Leakage current densities for the $(1-x)BiFeO_3-xAl_2O_3$ samples

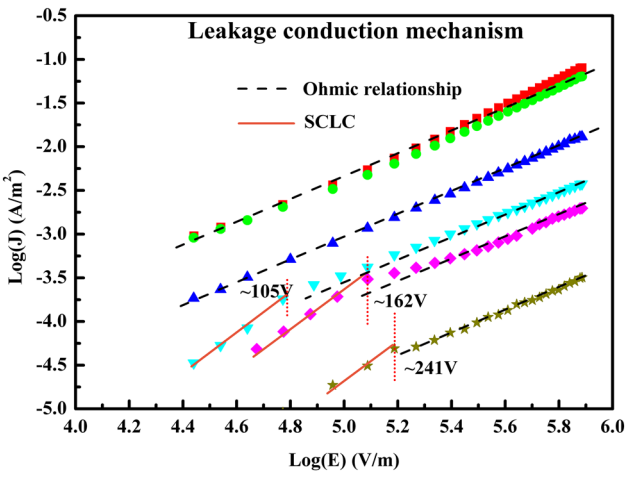

Fig. 6 Leakage current mechanisms for the $(1-x)BiFeO_3-xAl_2O_3$ samples

low voltage region, indicating a good agreement with SCLC theory [29]. Ramachandran et al. [30] and Ahn et al. [31] also found an SCLC conduction mechanism in $BiFeO_3$ system ceramics. As for A6, A8 and A10 samples, the voltage ranges affected by the SCLC mechanism increased monotonously into 105, 164, and 241 V, respectively, meaning that the SCLC mechanism tended to expand in leakage current characteristic.

The polarization hysteresis loops (P–E loops) measured for all the $(1-x)BiFeO_3-xAl_2O_3$ samples at room temperature are shown in Fig. 7. The polarization hysteresis loops were measured at different electric fields (10, 15 and 20 kV/cm) with an operating frequency of 100 Hz. The pure $BiFeO_3$ ceramic shown a leaky polarization hysteresis loop owing to its severe leakage current characteristics. This is very common in pure phase $BiFeO_3$ ceramics. However, the ferroelectric hysteresis loops became more typical in shape with the increase of the Al_2O_3 content, indicating that the leakage current density was decreased as discussed above. However, with the further addition of Al_2O_3, the value of remnant polarization decreased from 0.61 for A6 to 0.35 μC/cm^2 for A10, owing to the excessive addition of Al_2O_3 and the formation of secondary phase, which have no ferroelectric properties or lost ferroelectric properties above − 29 °C [18]. During the measurement process, it was hard to get an exact value of the saturated polarization hysteresis loops, owing to the electrical penetration of the samples occurred before full switching [32].

4 Conclusions

Lead-free $(1-x)BiFeO_3-xAl_2O_3$ composites ceramics were synthesized using the standard solid-state reaction method. The effects of Al_2O_3 addition on structural (crystal data and microstructure), leakage current characteristics, ferroelectric and dielectric properties of the $(1-x)BiFeO_3-xAl_2O_3$ composites were studied. Secondary phases ($Bi_2Fe_4O_9$ and $Bi_{24}Al_2O_{39}$) were increased with the addition of Al_2O_3. The average grain size significantly decreased from 1.49 μm

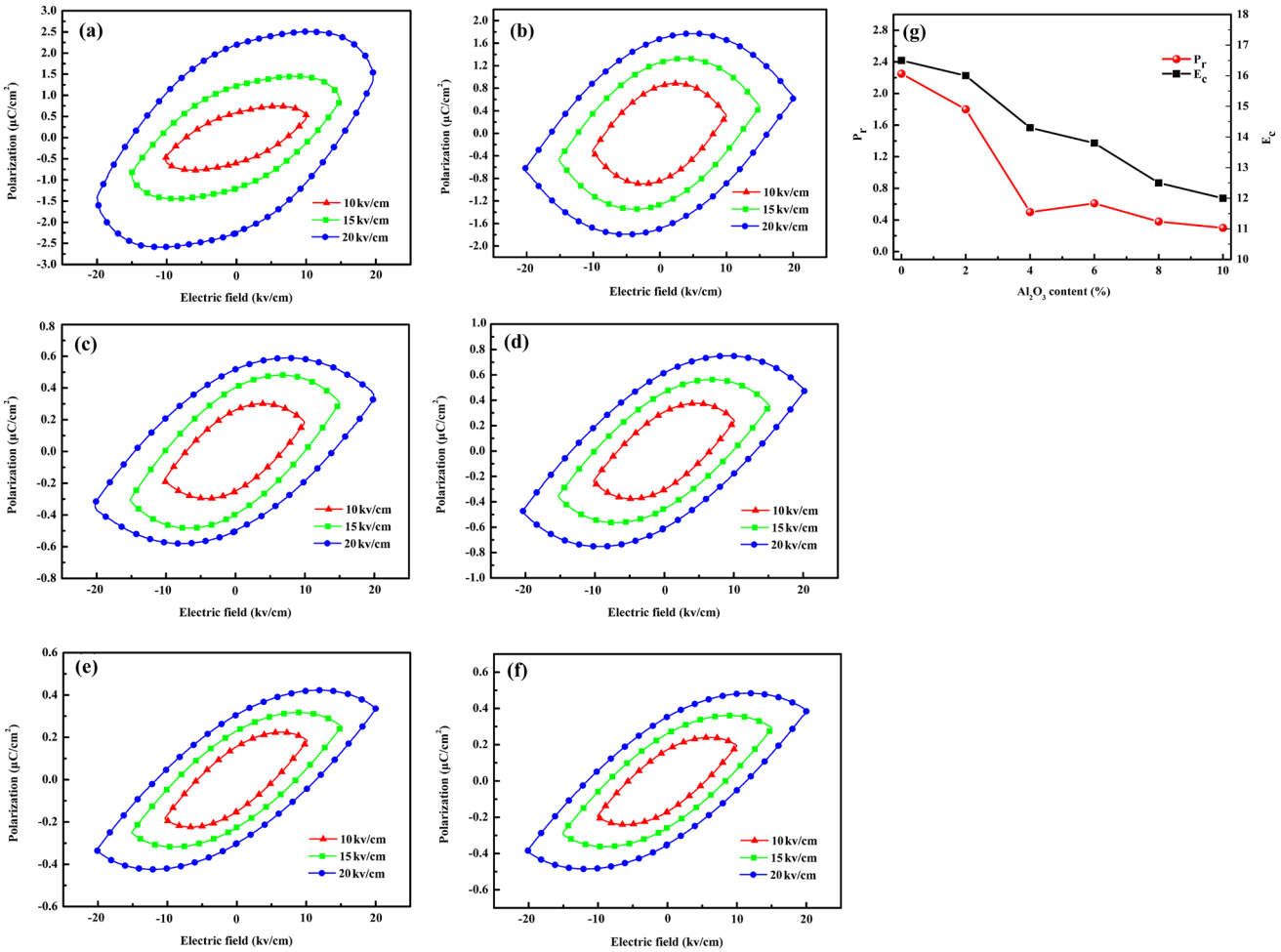

Fig. 7 P–E loops for the $(1-x)BiFeO_3-xAl_2O_3$ samples: **a** A 0, **b** A2, **c** A4, **d** A6, **e** A8, and **f** A10

for $x = 0.00$ to 0.45 μm for $x = 0.10$. The ceramics with the addition of Al_2O_3 showed smaller dielectric constant and dielectric loss compared with pure $BiFeO_3$ sample. The T_C decreased from 475 °C for A2 to 390 °C for A10. Leakage current density decreased significantly, and the leakage conduction mechanism was changed from Ohmic relationship to SCLC mechanism with the addition of Al_2O_3. In addition, the polarization hysteresis loops became more typical in shape with the increase of the Al_2O_3 content.

Acknowledgements This study has been supported by the fund of the Key New Product Project of Yunnan Province (Grant No. 2016BA009) and 2017 Kunming Advanced Talent Funding (13020163).

References

1. D. Lebeugle, D. Colson, A. Forget, M. Vire, Appl. Phys. Lett. **91**, 022907 (2007)
2. F. Yan, G. Zhao, N. Song, J. Alloys Comp. **570**, 19–22 (2013)
3. S.H. Song, Q.S. Zhu, L.Q. Weng, V.R. Mudinepalli, J. Eur. Ceram. Soc. **35**, 131–138 (2015)
4. F. Chang, N. Zhang, F. Yang, S. Wang, G. Song, J. Appl. Phys. **24**, 7799 (2007)
5. Y. Lee, J. Wu, C. Lai, Appl. Phys. Lett. **88**, 042903 (2006)
6. M. De, S.P. Patel, H.S. Tewari, J. Electron. Mater. **28**, 6928–6935 (2017)
7. A. Moure, J. Tartaj, C. Moure, J. Alloys Comp. **25**, 7042–7046 (2011)
8. G. Arlt, D. Hennings, G.D. With, J. Appl. Phys. **58**, 1619–1625 (1985)
9. Z.X. Cheng, A.H. Li, X.L. Wang, S.X. Dou, K. Ozawa, H. Kimura, S.J. Zhang, T.R. Shrout, J. Appl. Phys. **103**, 07E507 (2008)
10. S.F. Wang, G.O. Dayton, J. Am. Ceram. Soc. **82**, 2677–2682 (1999)
11. J. Zhuang, L. Su, W. Wu, H. Bokov, A.A. Liu, M. Ren, Appl. Phys. Lett. **107**, 182906 (2015)
12. Y. Wei, X. Wang, J. Zhu, X. Wang, J. Jia, J. Am. Ceram. Soc. **96**, 3163–3168 (2013)
13. D.S. Kim, J.H. Lee, R.J. Sung, W.K. Sang, H.S. Kim, J.S. Park, J. Eur. Ceram. Soc. **27**, 3629–3632 (2007)
14. A. Jawad, S. Arham, S. Ahmed, Z. Ashraf, M. Chaman, A. Azam, J. Alloys Comp. **530**, 63–70 (2012)
15. A. Azam, A. Jawad, A.S. Ahmed, M. Chaman, A.H. Naqvi, J. Alloys Comp. **509**, 2909–2913 (2011)
16. P. Bai, Y. Zeng, J. Han, Y. Wei, M. Li, Ceram. Int. **45**, 7730–7735 (2019)
17. S. Chandel, P. Thakur, S.S. Thakur, V. Kanwar, M. Tomar, V. Gupta, A. Thakur, Ceram. Int. **44**, 4711–4718 (2018)
18. T. Higashiwada, H. Asaoka, H. Hayashi, A. Kishimoto, J. Eur. Ceram. Soc. **27**, 2217–2222 (2017)
19. D. Wang, Z. Fan, D. Zhou, A. Khesro, S. Murakami, A. Feteira, J. Mater. Chem. A. **6**, 4133–4144 (2018)
20. H. Zheng, F. Straub, Q. Zhan, P. Yang, W. Hsieh, F. Zavaliche, Adv. Mater. **18**, 2747–2752 (2016)
21. H. Birey, J. Appl. Phys. **48**, 5209–5212 (1977)
22. S.R. Mohapatra, B. Sahu, T. Badapanda, M.S. Pattanaik, S.D. Kaushik, A.K. Singh, Ceram. Int. **1065**, 01574 (2016)
23. P. Sharma, S. Hajra, S. Sahoo, P.K. Rout, R. Choudhary, Appl. Ceram. **11**, 171–176 (2017)
24. S. Pattanayak, R.N.P. Choudhary, Ceram. Int. **41**, 9403–9410 (2015)
25. X.H. Liu, Z. Xu, S.B. Qu, X.Y. Wei, J.L. Chen, Ceram. Int. **34**, 797–801 (2008)
26. Z. Yue, G. Tan, W. Yang, H. Ren, A. Xia, Ceram. Int. **42**, 18692–18699 (2016)
27. J. Wei, Y. Liu, X. Bai, C. Li, Y. Liu, Z. Xu, Ceram. Int. **42**, 13395–13403 (2016)
28. H. Hu, S.B. Krupanidhi, J. Mater. Res. **9**, 1484–1498 (1994)
29. C.J. Peng, S.B. Krupanidhi, J. Mater. Res. **10**, 708–726 (1995)
30. B. Ramachandran, A. Dixit, R. Naik, G. Lawes, M.S. Ramachandra Rao, Phys Rev B. **82**, 012102 (2010)
31. K.H. Ahn, S.S. Kim, S.G. Baik, J. Appl. Phys. **92**, 421–425 (2002)
32. S. Dash, R. Padhee, P.R. Das, R.N.P. Choudhary, J. Mater. Sci.-Mater. Electron. **24**, 3315–3323 (2013)